

Supporting Information

for

Nanoscale capacitance spectroscopy based on multi-frequency electro-static force microscopy

Pascal N. Rohrbeck^{1,2}, Lukas D. Cavar^{1,3}, Franjo Weber^{1,2}, Peter G. Reichel¹, Mara Niebling^{1,3} and Stefan A. L. Weber^{*1,3,4}

Address: ¹Max Planck Institute for Polymer Research, Ackermannweg 10, 55128 Mainz, Germany;

²Department of Chemistry, University of Mainz, Duesbergweg 10-14, 55128 Mainz, Germany;

³Department of Physics, University of Mainz, Staudingerweg 7, 55128 Mainz, Germany and ⁴Institute for Photovoltaics, University of Stuttgart, Pfaffenwaldring 47, 70569 Stuttgart, Germany

Email: Stefan A. L. Weber - stefan.weber@mpip-mainz.mpg.de; Stefan.Weber@ipv.uni-stuttgart.de

* Corresponding author

Abbreviations

CPD	contact potential difference
H-SCM	heterodyne Scanning Capacitance Microscopy
EFM	Electrostatic Force Microscopy
F14H20	Perfluoroalkyl-Alkane $F(CF_2)_{14}(CH_2)_{20}H$
H-KPFM	Heterodyne Kelvin Probe Force Microscopy

Supporting Information

Supporting information features a comparison of the working principles of Heterodyne Kelvin Probe Force Microscopy (H-KPFM) and heterodyne Scanning Capacitance Microscopy (H-SCM), all the raw and normalized data of the H-SCM frequency spectroscopy, the full comparison of the H-SCM, SF-Electrostatic Force Microscopy (EFM), and H-KPFM images on the Perfluoroalkyl-Alkane $F(CF_2)_{14}(CH_2)_{20}H$ (F14H20) structures, and finally a comparison of the model data and the measured data on the microcapacitors.

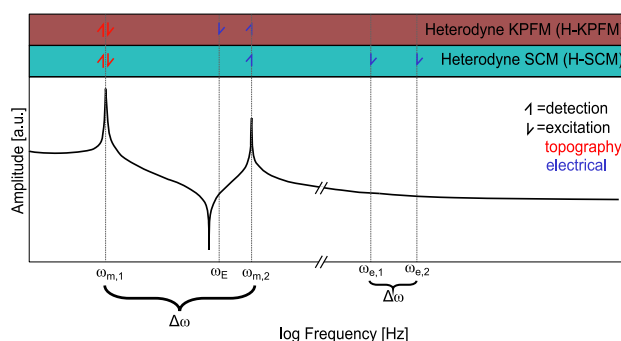


Figure S1: Schematic comparison of the excitation and detection frequencies in H-KPFM and H-SCM. The lower part shows the transfer function of the cantilever, where the amplitude is plotted vs the logarithmic angular frequency. The upper part shows the excitation frequencies (↓) and the detection frequencies (↑) of the applied frequencies. The red arrow corresponds to topography- and the blue arrow to the electrical signal. Representation of Fig. S1 was inspired by [1,2].

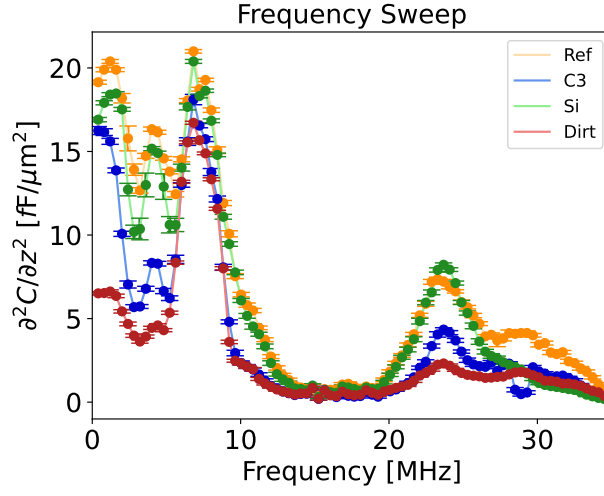


Figure S2: Non-normalized data of the comparison of the C'' frequency sweep shown in Figure 6 on the four spots while in H-SCM (see eq. (8)). This was conducted with the μ masch's HQ:NSC18/Pt cantilever.

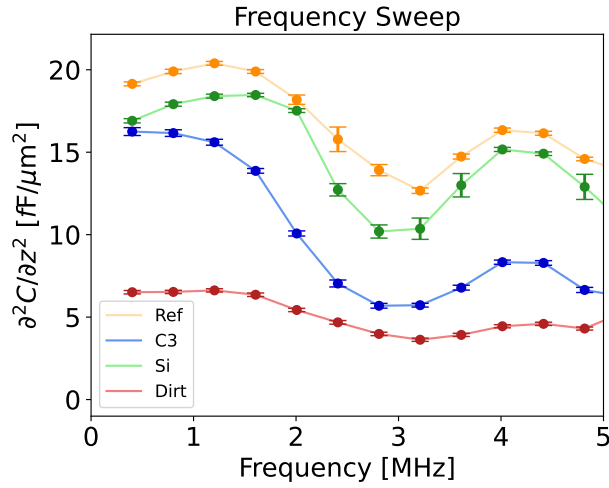


Figure S3: Zoom of the non-normalized data from the comparison of the C'' frequency sweep shown in Figure 6 on the four spots while in H-SCM (see eq. (8)). This was conducted with the μ masch's HQ:NSC18/Pt cantilever.

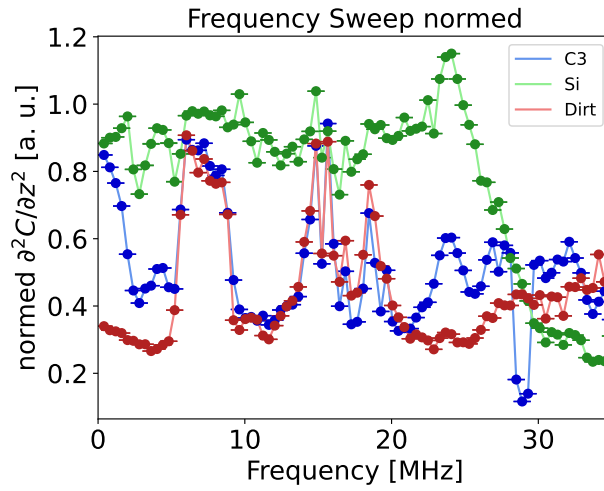


Figure S4: Normalized data of the C'' frequency sweep shown in Figure 6 on the three spots while in H-SCM (see eq. (8)). This was conducted with the μ masch's HQ:NSC18/Pt cantilever.

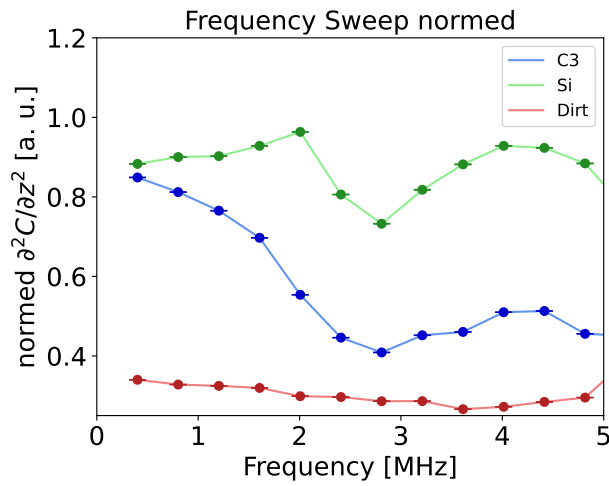


Figure S5: Zoomed and normalized data of the C'' frequency sweep shown in Figure 6 on the three spots while in H-SCM (see eq. (8)). This was conducted with the μ masch's HQ:NSC18/Pt cantilever.

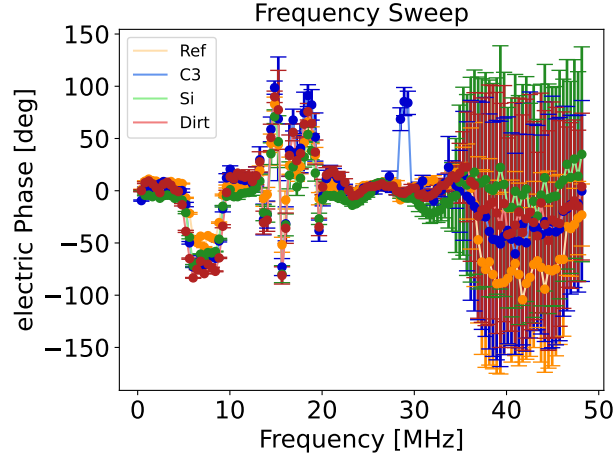


Figure S6: Non-normalized data of the phase signal φ spectra of the comparison from the C'' frequency sweep shown in Figure 6 on the four spots while in H-SCM (see eq. (8)). This was conducted with the μ masch's HQ:NSC18/Pt cantilever.

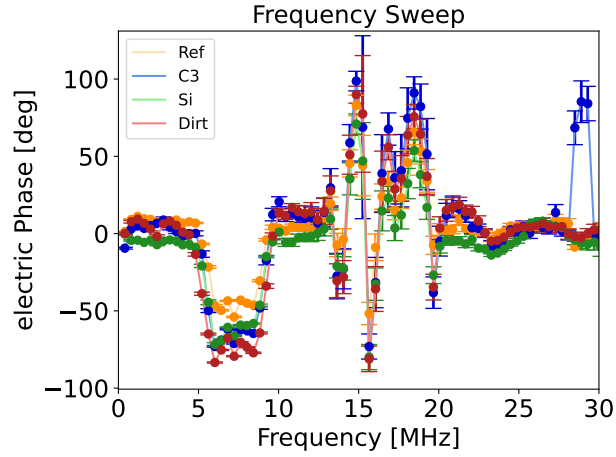


Figure S7: Zoom of the non-normalized data of the phase signal φ spectra of the comparison from the C'' frequency sweep shown in Figure 6 on the four spots while in H-SCM (see eq. (8)). This was conducted with the μ masch's HQ:NSC18/Pt cantilever.

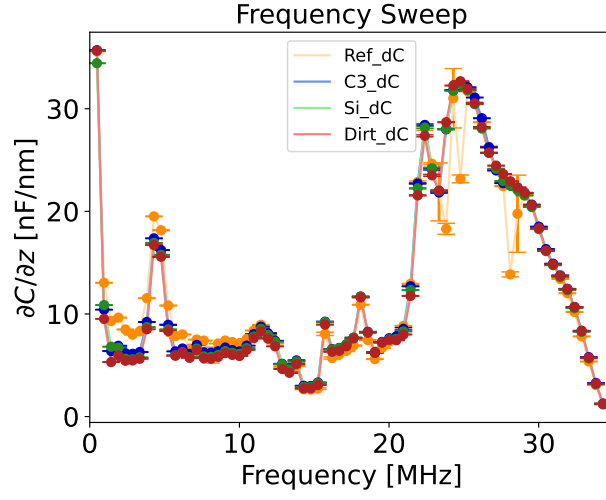


Figure S8: Non-normalized data of the comparison of the C' frequency sweep shown in Figure 6 on the four spots while in SF-EFM mode (see eq. (9)). This was conducted with the μ masch's HQ:NSC18/Pt cantilever.

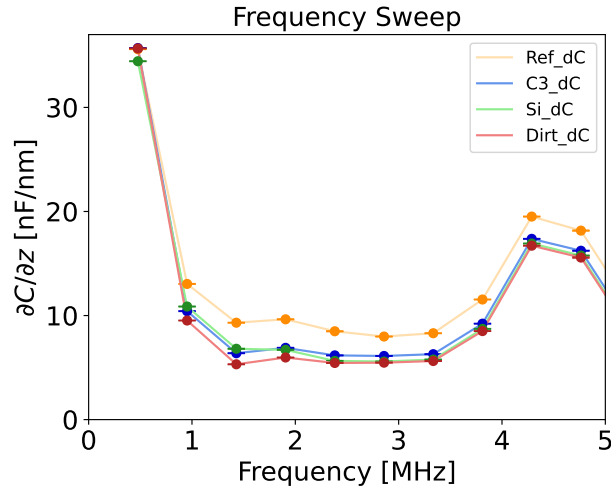


Figure S9: Zoom of the non-normalized data of the comparison of the C' frequency sweep shown in Figure 6 on the four spots while in SF-EFM mode (see eq. (9)). This was conducted with the μ masch's HQ:NSC18/Pt cantilever.

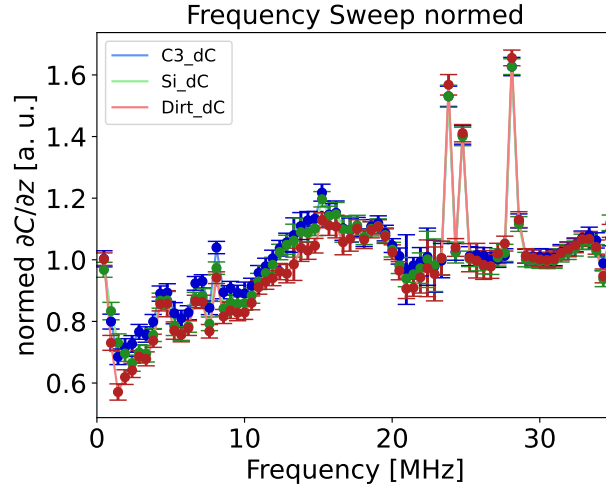


Figure S10: Normalized data of the C' frequency sweep shown in Figure 6 on the three spots while in SF-EFM mode (see eq. (9)). This was conducted with the μ masch's HQ:NSC18/Pt cantilever.

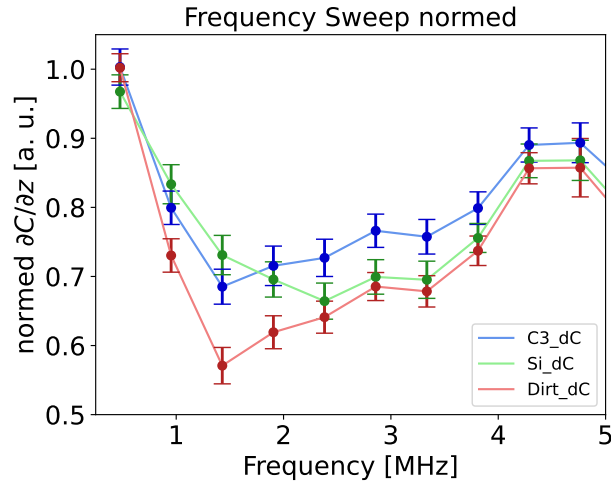


Figure S11: Zoomed and normalized data of the C' frequency sweep shown in Figure 6 on the three spots while in SF-EFM mode (see eq. (9)). This was conducted with the μ masch's HQ:NSC18/Pt cantilever.

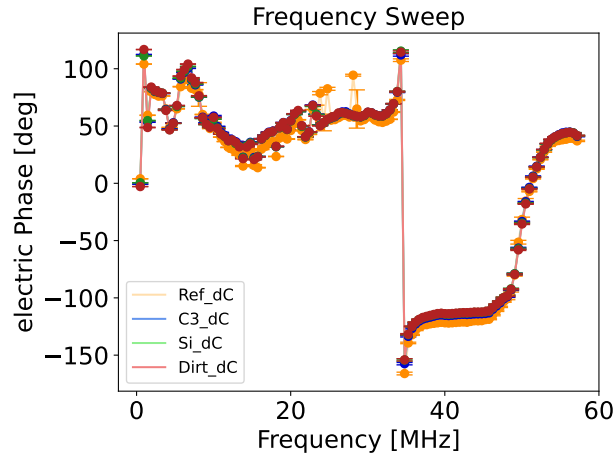


Figure S12: Non-normalized data of the phase signal φ spectra of the comparison of the C' frequency sweep shown in Figure 6 on the four spots while in SF-EFM mode (see eq. (9)). This was conducted with the μ masch's HQ:NSC18/Pt cantilever.

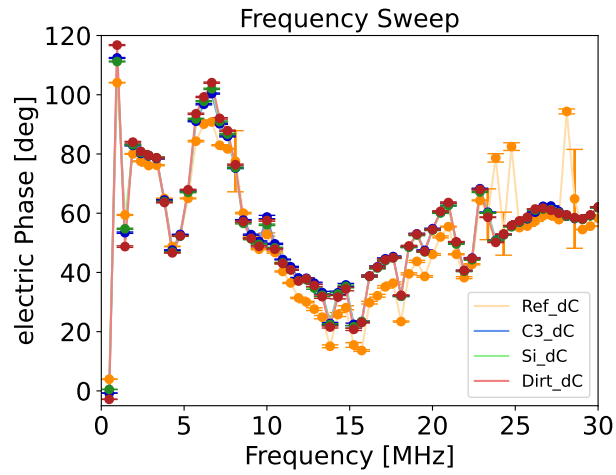


Figure S13: Zoom of the non-normalized data of the phase signal φ spectra of the comparison of the C' frequency sweep shown in Figure 6 on the four spots while in SF-EFM mode (see eq. (9)). This was conducted with the μ masch's HQ:NSC18/Pt cantilever.

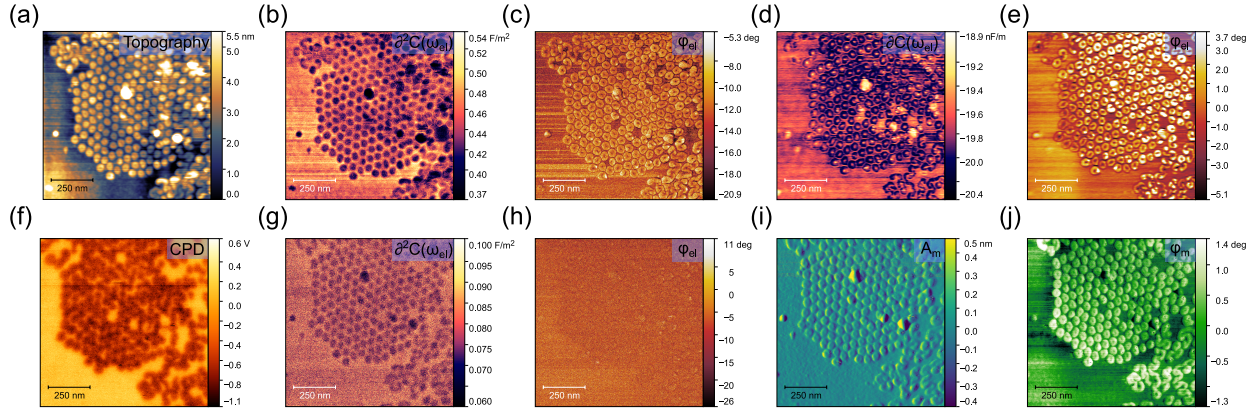


Figure S14: Full version of the H-SCM pictures given in Figure 7. H-SCM pictures made on F14H20 with (a) the topography, (b) the $C''(\partial^2 C)$ picture at 1.59 and 1.98 MHz, (c) electric phase ϕ_{el} of the $C''(\partial^2 C)$ signal at 1.59 and 1.98 MHz, (d) the $C'(\partial C)$ picture at 235.579 kHz, (e) electric phase ϕ_{el} of the $C'(\partial C)$ signal at 235.579 kHz, (f) the CPD picture, (g) the $C''(\partial^2 C)$ picture at 15.88 and 16.28 MHz, (h) electric phase ϕ_{el} of the $C''(\partial^2 C)$ signal at 15.88 and 16.28 MHz, (i) the picture of the mechanical amplitude at the resonance frequency of 74.580 kHz, and (j) the picture of the mechanical phase at the resonance frequency of 74.580 kHz. This was conducted with the μ masch's HQ:NSC18/Pt Cantilever.

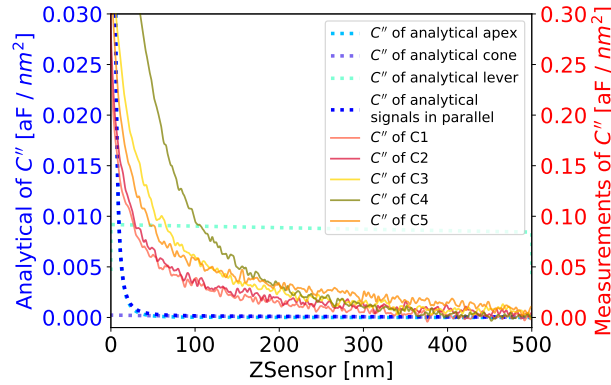


Figure S15: A comparison of the measured C'' values on various capacitors, as shown in Figure 2, is presented. The measurements, performed using the NuNano SPARK 70 Pt cantilever (solid lines), are contrasted with the theoretical contributions of the respective components to the first numerical derivative C' of the capacitance (dotted lines) as a function of the tip-to-sample distance, z . For the theoretical calculations, the properties of the NuNano SPARK 70 Pt cantilever ($w = 30 \mu\text{m}$, $l = 225 \mu\text{m}$, $\alpha = 11 \text{ deg}$, $h = 12 \mu\text{m}$, $\theta = 25 \text{ deg}$, $r = 18 \text{ nm}$, $\delta = 3.7 \cdot 10^{-7}$) with an mechanical amplitude of $A_m = 10 \text{ nm}$, an excitation voltage of $V_{AC} = 2 \text{ V}$, and a total amount of calculated points of 100,000, was used for these.

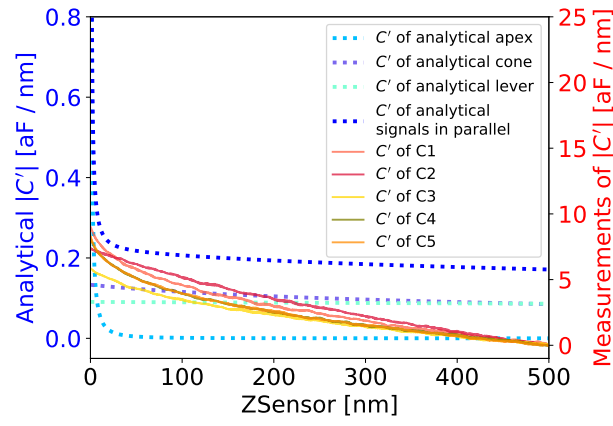


Figure S16: A comparison of the measured C' values on various capacitors, as shown in Figure 2, is presented. The measurements, performed using the NuNano SPARK 70 Pt cantilever (solid lines), are contrasted with the theoretical contributions of the respective components to the first numerical derivative C' of the capacitance (dotted lines) as a function of the tip-to-sample distance, z . For the theoretical calculations, the properties of the NuNano SPARK 70 Pt cantilever ($w = 30\text{ }\mu\text{m}$, $l = 225\text{ }\mu\text{m}$, $\alpha = 11\text{ deg}$, $h = 12\text{ }\mu\text{m}$, $\theta = 25\text{ deg}$, $r = 18\text{ nm}$, $\delta = 3.7 \cdot 10^{-7}$) with an mechanical amplitude of $A_m = 10\text{ nm}$, an excitation voltage of $V_{AC} = 2\text{ V}$, and a total amount of calculated points of 100,000, was used for these.

References

1. Garrett, J. L.; Munday, J. N. *Nanotechnology* **2016**, 27 (24), 14. doi:10.1088/0957-4484/27/24/245705.
2. Axt, A.; Hermes, I. M.; Bergmann, V. W.; Tausendpfund, N.; Weber, S. A. L. *Beilstein J. Nanotechnol.* **2018**, 9 (1), 1809–1819. doi:10.3762/bjnano.9.172.